New Aspects of Very High-Resolution Spaceborne SAR Image Formation

Pau Prats-Iraola, German Aerospace Center (DLR), Pau.Prats@dlr.de, Germany
Rolf Scheiber, German Aerospace Center (DLR), Rolf.Scheiber@dlr.de, Germany
Marc Rodriguez-Cassola, German Aerospace Center (DLR), Marc.Rodriguez@dlr.de, Germany
Francesco De Zan, German Aerospace Center (DLR), Francesco.DeZan@dlr.de, Germany
Andreas Reigber, German Aerospace Center (DLR), Andreas.Reigber@dlr.de, Germany
Alberto Moreira, German Aerospace Center (DLR), Alberto.Moreira@dlr.de, Germany

Abstract

This contribution addresses several important aspects that need to be considered for the processing of spaceborne SAR data with a resolution in the decimeter range (at X-band). In particular, it will be shown how the motion of the satellite during the transmission/reception of the chirp signal and the effect of the troposphere deteriorate the impulse response function if not properly considered. Further aspects that have been investigated include the curved orbit, the azimuth variance and the topography dependence. The focusing methodology is validated using simulated point targets and real data acquired by the TerraSAR-X satellite in the staring spotlight mode.

1 Introduction

Spaceborne SAR processing is already an established topic. Many efficient solutions have been proposed over the last decades for every imaging mode, be it stripmap, spotlight, ScanSAR or TOPS (Terrain Observation by Progressive Scans). However, the assumptions of some of these algorithms start to be invalid depending on the acquisition geometry, especially in terms of the image resolution. While airborne SAR processors achieve nowadays a resolution in the decimeter range, the same approaches do not perform perfectly in a low Earth orbit (LEO) scenario, mainly due to the much greater sensor velocity and the larger distances involved. Furthermore, when getting close to decimeter resolution (at X-band) several effects appear, which do not show up in an airborne scenario and must be taken into account to achieve a satisfactory focusing performance.

The first of these effects occurs due to the motion of the satellite *during* the transmission and reception of the chirp signal. This effect is well-known in the frame of frequency-modulated continuous-wave (FMCW) SAR radars mounted on airborne platforms [1]. In Section 2.1, the impact on high-resolution pulsed radars is analyzed. The curved orbit and the validity of the hyperbolic approximation is also a topic that has been addressed before in the literature [2, 3]. Section 2.2 suggests an innovative correction of the orbit curvature based on state-of-the-art airborne SAR motion compensation techniques. A discussion on the azimuth variance of the spaceborne geometry is also included. A further aspect is the delay introduced by the troposphere in the range history. This delay can change significantly due to the variation of the squint (or azimuth) angle during the formation of the synthetic aperture, hence resulting in azimuth defocusing if not considered, especially at higher frequency bands. Section 2.3 addresses this topic and suggests a model-based correction. A final aspect is the topography dependence of the focusing kernel due to the curved orbit, which is addressed in Section 2.4. Finally, Section 3 presents some results including point-target simulations to validate the proposed approaches.

2 Key Aspects of Very High-Resolution Spaceborne SAR

2.1 The Stop-and-Go Effect

In the processing of spaceborne SAR raw data it is usually assumed that the platform does not move during the transmission of the pulse signal and the reception of the backscattered echoes. Such an assumption is usually called the stop-and-go or start-stop approximation and has mainly two effects. A "slow-time" one, which is linked to the fact that the satellite indeed moved between transmission and reception, e.g., about $30\ \mathrm{m}$ in the TerraSAR-X (TSX) case. This fact implies mainly a range-dependent azimuth shift of the focused signal, which can be efficiently considered with a linear azimuth phase ramp in the range-Doppler domain after the range cell migration correction (RCMC) [4]. A second effect deals with the motion of the satellite during the transmission and reception of the chirp signal itself, i.e., a "fast-time" effect or, in other words, a real Doppler effect. The TSX chirp signal has a length of about $50\ \mu\mathrm{s}$, during which the satellite moves about $40\ \mathrm{cm}$ in the azimuth direction. This effect is well-known in FMCW SAR systems [1]. The phenomenon was also discussed in [5] for pulsed radars, where the analysis was done in terms of a mismatch during the matched filtering in range. As shown in [5], the difference in the instan-

taneous frequency between the nominal range variation and the one including the motion of the platform is given by the Doppler centroid, f_{DC}, caused by the platform movement during transmission/reception. By assuming a large time-bandwidth product, the shift in the signal in the range-time dimension is then given by $f_{\mathrm{DC}}/K_{\mathrm{r}}$, being K_{r} the chirp rate. This means that there is a range shift present in the signal as a function of the instantaneous azimuth frequency. In the case of large azimuth bandwidths, this effect will introduce different range shifts along the azimuth integration interval, hence deteriorating the impulse response function in both dimensions. Another intuitive way to visualize this effect is by considering different azimuth phase ramps as a function of the range frequency, since, due to the large time-bandwidth product, there is a direct mapping between fast-time and range frequency. In other words, due to the motion of the satellite, the zero-Doppler time changes as a function of the range frequency, corresponding to a range-frequency dependent linear phase ramp in the azimuth dimension.

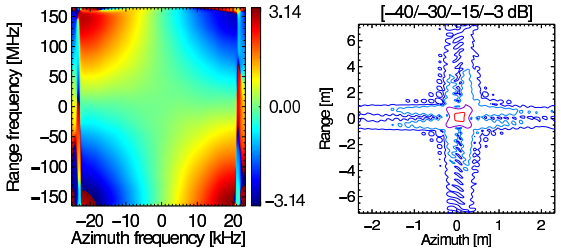

Figure 1: Effect of the stop-and-go approximation in the TSX staring spotlight (ST) mode. (Left) Residual phase in radians of a CR in the 2D frequency domain, and (right) the corresponding contour plot of the oversampled IRF. The chirp length is $50\ \mu$s, the bandwidth 300 MHz, and the azimuth processed band
width 38.5 kHz.

Figure 1 shows the resulting phase error due to the stop-and-go approximation measured over a corner reflector (CR) of a TSX staring spotlight (ST) acquisition and the corresponding impulse response function (IRF). The first plot on the left is the phase of the 2D phase spectrum after removing the global linear ramps due to the target position. The error reaches $\pm 177^{\circ}$ at the edges of the spectrum. If not corrected, this error introduces resolution loss of up to 15% in both dimensions for an azimuth bandwidth of 38.5 kHz (16 cm resolution without weighting), a range bandwidth of 300 MHz and a chirp length of $50\,\mu$s. Since the effect is space invariant, it can be easily corrected in the 2D frequency domain using the following phase function [1, 7]

$$H_{\mathrm{ss}}^{\mathrm{fast}}(f_{\mathrm{a}}, f_{\mathrm{r}}) = \exp\left[\mathrm{j}\cdot 2\pi \cdot \frac{f_{\mathrm{a}}}{K_{\mathrm{r}}} \cdot f_{\mathrm{r}}\right]. \qquad (1)$$

This phase correction shall be applied at the beginning of the processing before calling the focusing kernel.

2.2 The Curved Orbit

A hyperbolic range history, i.e., a linear track, is assumed by most spaceborne SAR image formation algorithms, but this approximation becomes less accurate the larger the integration time. For example, the TSX ST mode has an integration time of about 7 seconds, which can introduce errors of more than 200° at the edge of the synthetic aperture, resulting in a severe degradation of the IRF. Some solutions exist in the literature that use a numerical approach to circumvent this problem, e.g. [2, 3]. Also in the present case a numerical approach has been selected, which resembles the motion compensation approach in airborne SAR systems. The line-of-sight (LOS) approximation error, δr_{hyp}, can be computed for a reference target in the middle of the scene, yielding

$$\begin{aligned}\delta r_{\mathrm{hyp}}(t; r_{\mathrm{ref}}) \;=\; & \frac{1}{2}\cdot\Big[\,|\mathbf{p}_{\mathrm{sat}}^{\mathrm{Tx}}(t) - \mathbf{p}_{\mathrm{bc}}(t; r_{\mathrm{ref}})| \\ & + |\mathbf{p}_{\mathrm{sat}}^{\mathrm{Rx}}(t) - \mathbf{p}_{\mathrm{bc}}(t; r_{\mathrm{ref}})|\,\Big] \\ & - \sqrt{r_{\mathrm{ref}}^2 + v_{\mathrm{e,ref}}^2(t; r_{\mathrm{ref}})\cdot(t-t_0)^2},\end{aligned} \qquad (2)$$

where t is the azimuth time, t_0 and $v_{\mathrm{e,ref}}$ are the zero-Doppler time and the effective velocity for the reference point, respectively. $\mathbf{p}_{\mathrm{sat}}$ is the satellite position vector and the superscripts Tx and Rx indicate the different positions at transmission and reception, respectively, i.e., the bistatic character of the survey is accounted for. The target at the center of the beam is indicated by the vector $\mathbf{p}_{\mathrm{bc}}$, where the dependence with time indicates that the reference target might change in time, as for example occurs in the sliding spotlight mode.

Every echo line can be shifted in terms of range and phase as given by $\delta r_{\mathrm{hyp}}[n; r_{\mathrm{ref}}]$ using a phase ramp in the range frequency domain, where n corresponds now to the discrete azimuth time or echo line [7]. The above displacement can be corrected either in the range-Doppler domain or in the azimuth-time domain. The former performs the correction perfectly matched to the point in the middle of the beam, while the latter approximates the compensation optimally to a line at mid-range. While the first option neglects the azimuth variance of the geometry, the second one partially corrects it. Indeed, the correction in the azimuth-time domain can accommodate the azimuth variance besides correcting the non-hyperbolic term due to the small beamwidth of the antenna. This correction makes the beam-center approximation, i.e., the correction is only valid for the target in the middle of the beam, but given the small beamwidth of current spaceborne sensors, e.g., 0.33° for TSX, the introduced error is very small. After applying the correction, a pure hyperbolic phase history is forced, so that a conventional frequency domain kernel assuming a hyperbolic phase history can still be used to process the data without modifications. Note that this correction is accurate in wide-bandwidth terms, but only for the reference target. Therefore, for other ranges or azimuth positions the correction becomes less accurate the larger the scene size, which can be overcome by using a second-order orbit compensation (OCO), as also performed with airborne SAR systems.

A numerical simulation using a TSX-like orbit was performed in order to evaluate the azimuth-variant geometry, occurring due to the curved orbit and Earth's rotation, for different incidence angles and latitudes. **Figure 2** shows the quadratic phase error (QPE) at the edge of the azimuth processed bandwidth, which in this case corresponds to 15 cm azimuth resolution without weighting. The analyzed target is located 2 km away from the reference target in the azimuth dimension, but at the same slant-range. Note that the given values vary linearly with the distance to the scene center, quadratically with the azimuth processed bandwidth and linearly with the wavelength. Note also that due to the spotlight acquisition geometry, it does not help to process the raw data in azimuth blocks to accommodate the azimuth variance. When correcting the curved orbit using (2) the phase errors remain smaller than 2° at all latitudes and ranges (see [7]).

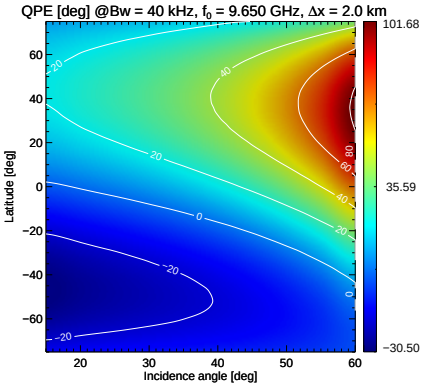

Figure 2: Quadratic phase error (QPE) in degrees at the edge of the azimuth processed bandwidth due to the azimuth variance of the imaging geometry as a function of the incident angle and the latitude. A Keplerian TSX-like orbit was simulated.

2.3 Tropospheric Effects

The troposphere introduces an undesired delay in the electromagnetic signal in the order of $2-4$ meters (one-way). The zenith path delay through the troposphere as a function of the target height has been modeled in the literature in different ways, e.g., using a quadratic or an exponential function. The operational TSX processor uses the latter model [4], which is given by

$$\Delta R_{\text{tropo}}(t; r_{\text{ref}}) = \frac{Z \cdot \exp\left[-h(r_{\text{ref}})/H\right]}{\cos\theta(r_{\text{ref}}) \cdot \cos\alpha(t; r_{\text{ref}})}, \quad (3)$$

where Z is a constant zenith path delay in meters, H is the thickness assumed for the troposphere, h is the altitude of the target, θ is the off-nadir angle, and α, which has been introduced here in addition, is the instantaneous azimuth angle within the formation of the synthetic aperture. The presented model is physically valid for a homogeneous troposphere layer within the synthetic aperture. For the purpose of correct focusing, it suffices to know the zenith path delay Z with decimeter accuracy. **Figure 3** plots (3) after subtracting a constant offset, as a function of the azimuth angle α assuming the following values: $H = 6$ km, $Z = 2.6$ m, $h = 629$ m and $\theta = 35^\circ$. As it can be induced from Figure 3, for large integration times the dependence with α is not negligible, hence introducing defocusing and phase errors if not considered. Furthermore, the delay in absolute terms, which in the TSX case shifts the image about 6 pixels in the slant-range dimension for the maximum sampling frequency, implies a mis-match of the azimuth compression filter, introducing additional defocusing and phase errors.

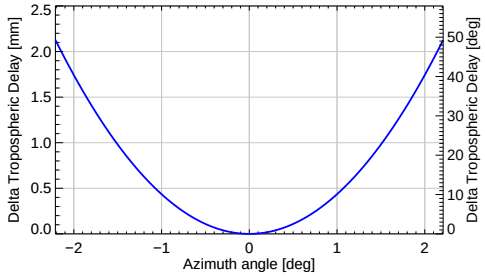

Figure 3: Delta tropospheric delay, i.e., after subtracting a constant offset, as a function of the azimuth angle using (3). The angle variation corresponds to the TSX ST mode. If not considered, the phase error will turn into azimuth defocusing and phase errors.

For the configuration of the TSX data take over Oberpfaffenhofen (see [7]), the troposphere introduces a quadratic error of about 50° at the edge of the processed bandwidth, and the further 50° occur due to the azimuth filter mismatch, resulting in a total of 100°, which degrades the azimuth resolution by about 10%. The correction of the troposphere using (3) can be applied together with the first order OCO, since a bulk correction for the middle of the scene suffices.

2.4 Topography Dependence

For a given zero-Doppler slant-range distance r_0, the range history in a spaceborne scenario depends on the topography due to the curved orbit. Similar as with the hyperbolic range history approximation, this effect becomes more noticeable for larger integration times. This means that, if the processing is performed with an azimuth-invariant reference height, as is usually assumed within current spaceborne imaging algorithms, azimuth defocusing might occur. **Figure 4** shows the height error that results in a phase error of $\pi/2$ at the edge of the processed bandwidth as a function of the azimuth resolution for the TSX-like orbit. This corresponds to a resolution loss of approximately 10% without weighting function, since the phase error is mainly quadratic with frequency. In the TSX staring spotlight mode the topography should be known with an accuracy better than 60 m in order to avoid a defocusing greater than 10%.

Due to the space variance of this effect, it is not trivial to include the compensation within the kernel of a Fourier-based processor. Therefore, one straightforward approach is to perform a block-wise post-focusing using an external DEM as suggested in [6]. Please note that for the results shown in Section 3, no post-focusing was performed and instead the reference height was matched to that of the reference points to be analyzed.

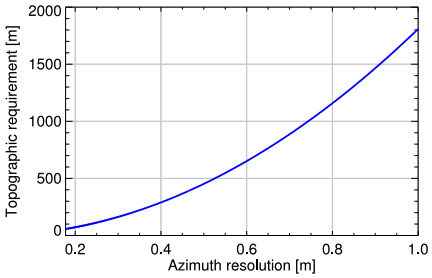

Figure 4: Maximum allowed topographic height error as a function of the azimuth resolution by allowing a maximum phase error of $\pi/2$ at the edge of the azimuth processed bandwidth. A TSX-like orbit has been simulated.

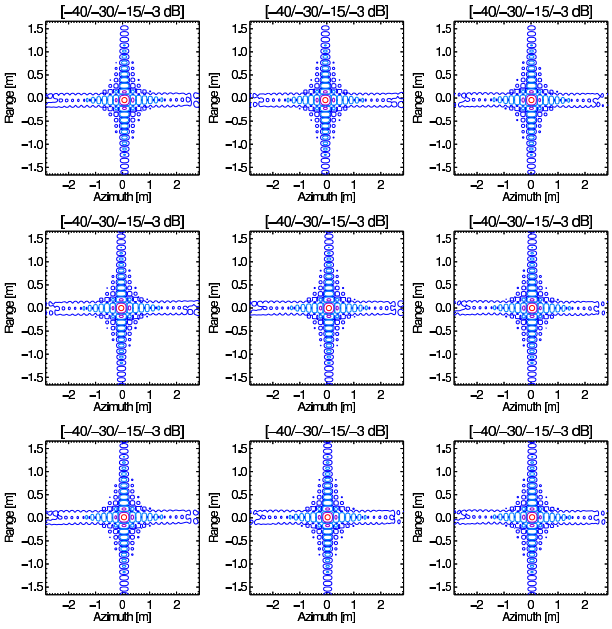

Figure 5: Contour plots of the interpolated IRFs by using the proposed processing chain with the extended ω-k (EOK).

3 Experimental Results

A simulation with point targets was performed using the following parameters: X-band, 33 kHz azimuth processed bandwidth (19 cm unweighted), 1.2 GHz chirp bandwidth and scene size of 5 km×5 km. The motion of the satellite was simulated between and during transmission and reception. Due to the large relative bandwidth, monochromatic algorithms do not perform properly, so the EOK approach was selected [8], further including a residual RCMC in the form of an interpolation in the range-Doppler domain after the Stolt mapping to adapt for the variation of the effective velocity [7]. The stop-and-go correction [eq. (1)] and the first-order OCO including (2) and (3) have been applied. No topography correction was applied as described in [6], since all the simulated targets are at the reference height. **Figure 5** shows the IRFs of the nine point targets, which are located at the edges and the center of the scene. The measured resolutions are within 0.5% accuracy while the interferometric phase errors are smaller than 1°. The proposed approaches were also validated using TSX staring spotlight data with an unweighted azimuth resolution of 16 cm [7]. **Figure 6** shows the IRF of a corner reflector in this TSX staring spotlight data take with and without the suggested corrections. Without these corrections the resolution loss in both dimensions is more than 50%.

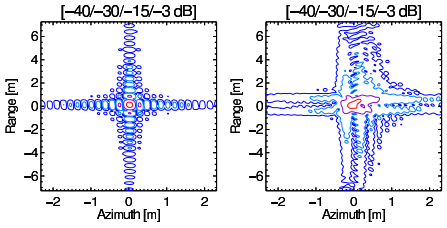

Figure 6: Contour plots of the interpolated IRF of a CR in a TSX staring spotlight acquisition after processing (left) with and without (right) the proposed corrections.

4 Conclusions

This paper has presented new aspects that need to be considered in the processing of very high-resolution spaceborne SAR data. Fore each one a solution has been proposed, and results with simulated point targets and with real TSX data have been included to validate the suggested solutions.

References

[1] A. Meta *et.al.*, *Signal processing for FMCW SAR*, IEEE Trans. Geosci. Remote Sens., vol. 45, no. 11, Nov. 2007

[2] K. Eldhuset, *A new fourth-order processing algorithm for spaceborne SAR*, IEEE Trans. Aero. Elec. Sys., vol. 34, no. 3, 1998

[3] D. D'Aria *et.al.*, *High-resolution spaceborne SAR focusing by SVD-Stolt*, IEEE Geosci. Remote Sens. Lett., vol. 4, no. 4, Oct. 2007

[4] H. Breit *et.al.*, *TerraSAR-X SAR processing and products*, IEEE Trans. Geosci. Remote Sens., vol. 48, no. 2, Feb. 2010

[5] J. C. Curlander *et.al.*, *Synthetic Aperture Radar: Systems and Signal Processing*, New York, USA: John Wiley & Sons, 1991

[6] M. Rodriguez-Cassola *et.al.*, *Doppler-related focusing aspects in the TOPS imaging mode*, Proc. IGARSS, Melbourne, Australia, 2013

[7] P. Prats-Iraola *et.al.*, *On the processing of very high resolution spaceborne SAR data*, , IEEE Trans. Geosci. Remote Sens., *accepted*, 2014

[8] A. Reigber *et.al.*, *Extended wavenumber domain SAR focusing with integrated motion compensation*, IEE Proc. Radar Sonar Navig., vol. 153, no. 3, 2006